Electronic Supplementary Material (ESI) for Journal of Materials Chemistry C.
This journal is © The Royal Society of Chemistry 2021

Supplemental Material
for

Cage Boron Allotrope with High Superconductivity at Ambient Pressure

Yiwei Liang[1], Meiling Xu[*1], Ziyang Qu[1], Shuyi Lin[1], Jian Hao[1], Yinwei Li [*1,2]

[1]Laboratory of Quantum Functional Materials Design and Application, School of Physics and Electronic Engineering, Jiangsu Normal University, Xuzhou 221116, China

[2]Shandong Key Laboratory of Optical Communication Science and Technology, School of Physical Science & Information Technology of Liaocheng University, Liaocheng 252059, China

To whom all correspondence should be addressed.
xml@calypso.cn and yinwei_li@jsnu.edu.cn

Computational Details

Our structural prediction approach is based on a global minimization of free energy surfaces of given compounds by combining *ab initio* total-energy calculations with particle swarm optimization (PSO) methodology. The structure search of MnB_{12} is performed with simulation cells containing 1 - 4 formula units (f.u.) at 30 GPa. In the first generation, the structures are randomly produced with certain symmetry that atomic coordinates can be generated by the crystallographic symmetry operations. The local optimizations of candidate structures are done by using the conjugate gradients method through Vienna *ab initio* simulations package (VASP), and stopped when an energy convergence threshold is smaller than 1×10^{-4} eV per cell. The next generation is constructed by 60% of the structure processed from the previous generation that is selected the lower energies by PSO, and other 40% of the structures is produced randomly. The structure fingerprinting technique of bond characterization matrix is applied to prohibition the production of similar structures, which is prominent augment the diversity and make the structural global search efficiency. For most of cases, the structure search for each chemical composition converges (evidenced by no structure with the lower energy emerging) after 1500 ~ 2000 structures investigated (i.e. in about 30 ~ 40 generations). In order to further search for low-lying structures, we select ten structures that have lower total energies, then use the density functional theory as implemented in the VASP code to perform structural optimization.

Our first-principles calculations were carried out using the density functional theory as implemented in the VASP code, adopting the all-electron projector-augment wave methods[1], with $2s^22p^1$ and $3d^64s^1$ treated as valence electrons for Mn and B, respectively, and the Perdew, Burke, and Ernzerhof exchange-correlation functional in the generalized gradient approximation[2]. A cutoff energy of 500 eV and fine Monkhorst-Pack *k* meshes[3] were chosen for ensuring residual forces are smaller than 10^{-3} eV/Å. This optimization's total energies were converged within ~1 meV/atom.

The formation energy (ΔG_f) that relative to the hcp Mn and α-B_{12} solids elemental was calculated at each considered pressure and temperature according to the equation below:

$$\Delta G_f(MnB_{12}) = \left[G(MnB_{12}) - G(Mn) - 12G(B)\right]/13,$$

where ΔG_f is the formation energy and G is the total Gibbs free energy of each structure and. In this formula $G = U + PV - TS$, the G is Gibbs free energy, the U is internal energy, the P is pressure, the V is volume, the T is temperature and the S is entropy.

The formation enthalpies of MnB_{12} phases as function of temperatures were calculated, where the temperature effects are considered by calculating the vibrational entropy by using quasi-harmonic approximation. we have performed two sets of calculations. First, we calculated the phonon dispersions and the corresponding phonon density of states (PDOS) using the direct supercell method as implemented PHONOPY code, and used the obtained PDOS as input to evaluate the vibrational contribution to the entropy of each phase. The Gibbs free energies of the relevant phases can be computed by combining with the total internal energy, pressure and volume obtained from the VASP calculations.

First-principles molecular dynamics (MD) simulations using the canonical *NVT* (*N* is the number of particles, *V* is volume, and *T* is temperature) are performed with 3×3×2 supercell with a time step of 1fs and the total simulation time is 20 ps.

The integrated crystal orbital Hamilton populations (ICOHP) are performed as implemented in the LOSBSTER code[4,5] to analyze the relative bond strength between B-B and Mn-B.

Through the QUANTUM ESPRESSO code, we calculated Electron-phonon coupling (EPC) of the compounds within the linear-response theory framework. The pseudopotentials for Mn and B elements are used USPP with a kinetic cutoff energy of 90 Ry. The *q* mesh of 6×6×6 (18 *q* points) and 8×8×8 (75 *q* points) for the *P*4/*mmm* MnB_{12} and *P*4/*mmm* B_6 in the first Brillouin zone are used in the EPC calculations. Correspondingly, the *k* mesh of 24×24×42 and 32×32×32 in the first Brillouin are used to for *P*4/*mmm* MnB_{12} and *P*4/*mmm* B_6, respectively. The 5×5×5, 5×5×5, 7×7×7, and 6×6×6 q meshes in the first Brillouin are used for *Pm*_1, *P*1, *P*2/*m*, and *Pm*_2, respectively. And the corresponding *k* meshes was 20×20×20, 20×20×20, 28×28×28, and 24×24×24.

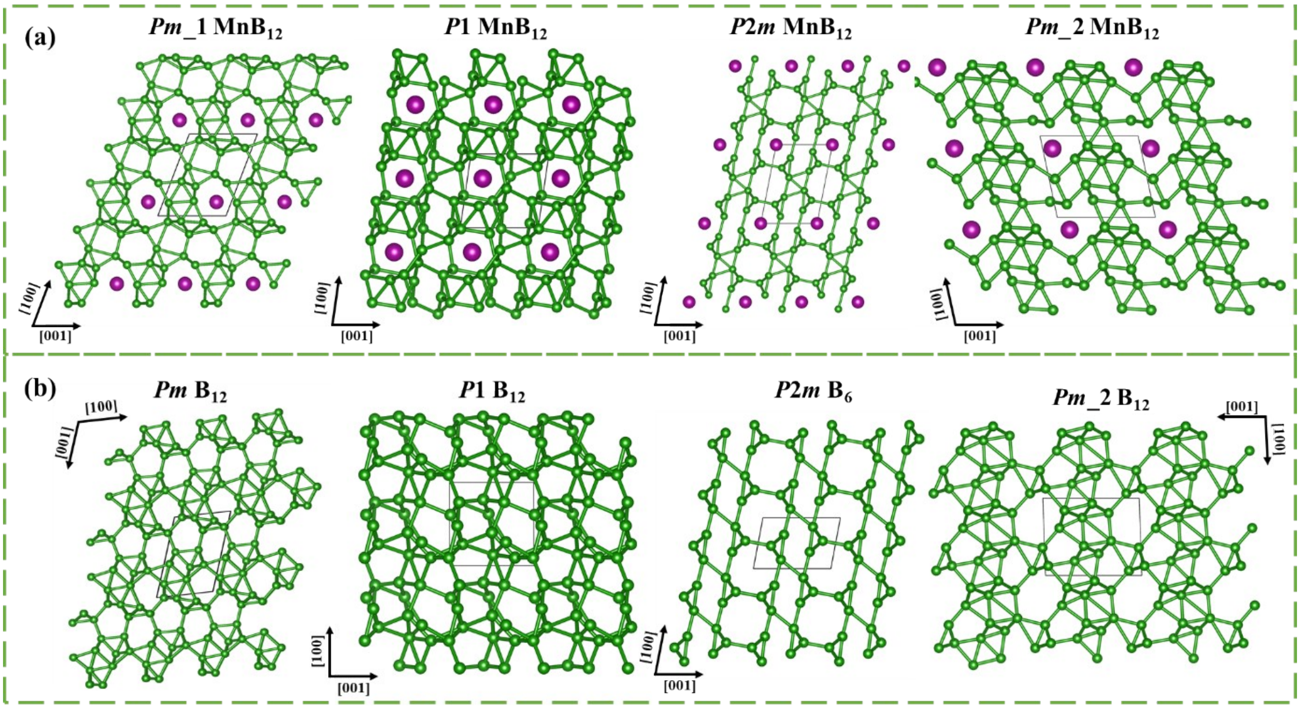

Figure S1 (a). The crystal structures of *Pm*_1, *P*1, *P*2/*m*, and *Pm*_2 MnB_{12} at zero pressure. (b) The crystal structures of *Pm*_1 B_{12}, *P*1 B_{12}, *P*2/*m* B_6 and *Pm*_2 B_{12} at zero pressure.

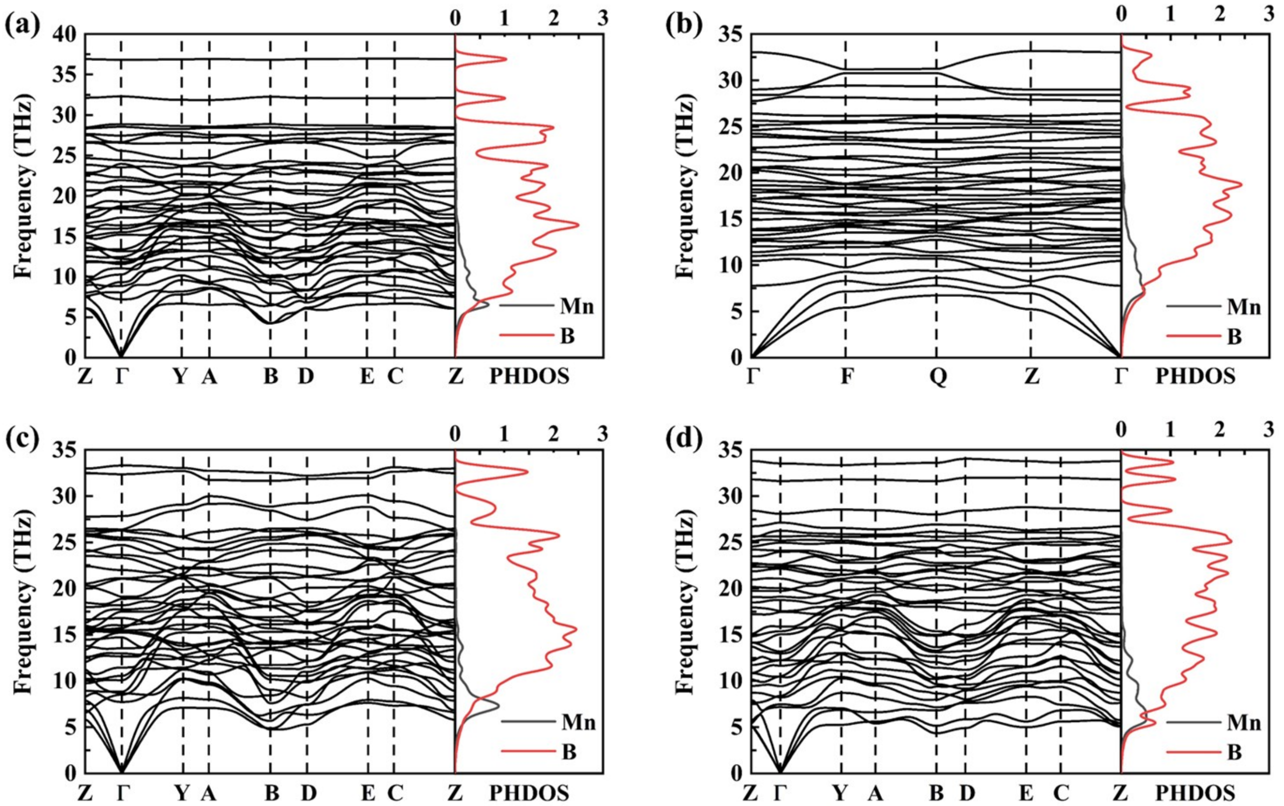

Figure S2. Phonon dispersions and phonon density of states (PhDOS) of (a) *Pm*_1, (b) *P*1, (c) *P*2/*m* and (d) *Pm*_2 MnB_{12} at 0 Gpa.

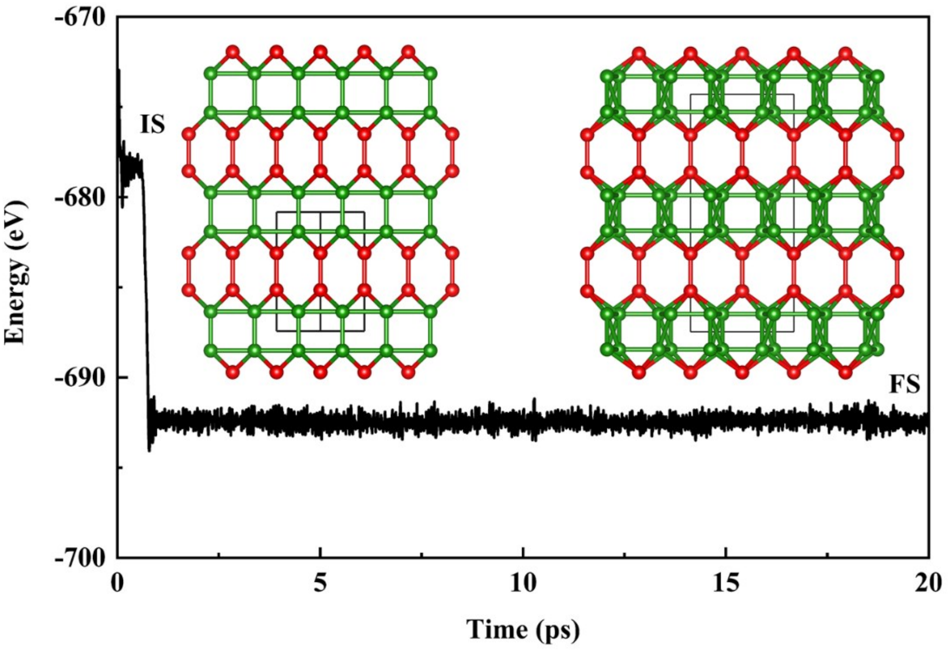

Figure S3. Evolution of relative energies during MD simulation. The insets are snapshots of structures at the first state and final state.

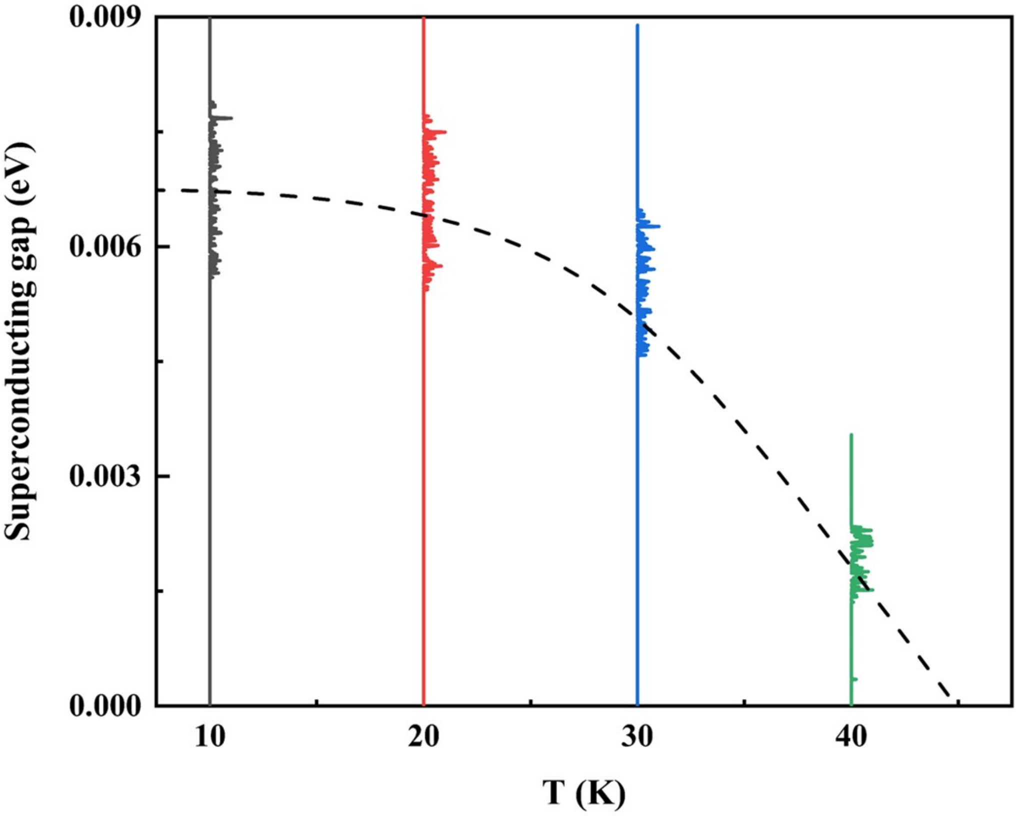

Figure S4. Calculated anisotropic superconducting gap as a function of temperature in *t*-B.

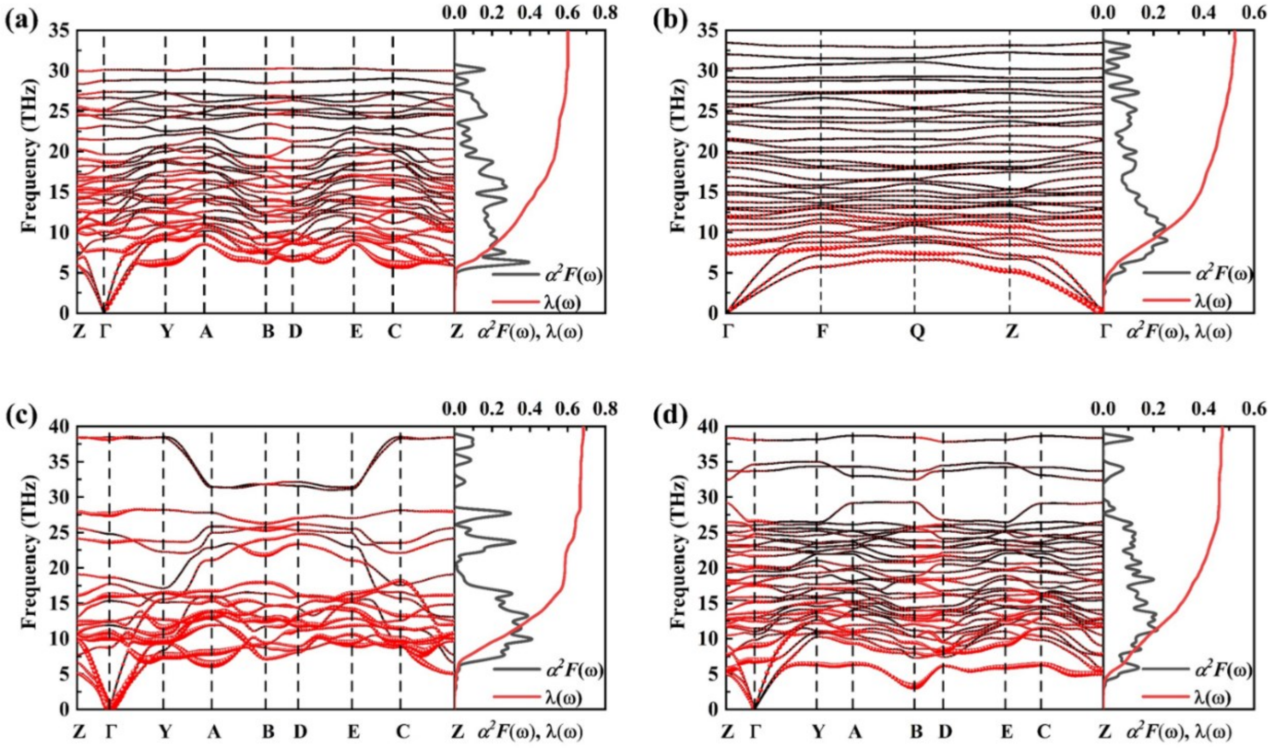

Figure S5. Phonon dispersions, Eliashberg function $\alpha^2F(\omega)$ and integrated electron–phonon coupling strength $\lambda(\omega)$ of (a) *Pm*_1 B_{12}, (b) *P*1 B_{12}, (c) *P*2/*m* B_6 and (d) *Pm*_2 B_{12} at 0 GPa. The magnitude of $\lambda(\omega)$ is indicated by the size of red ribbons.

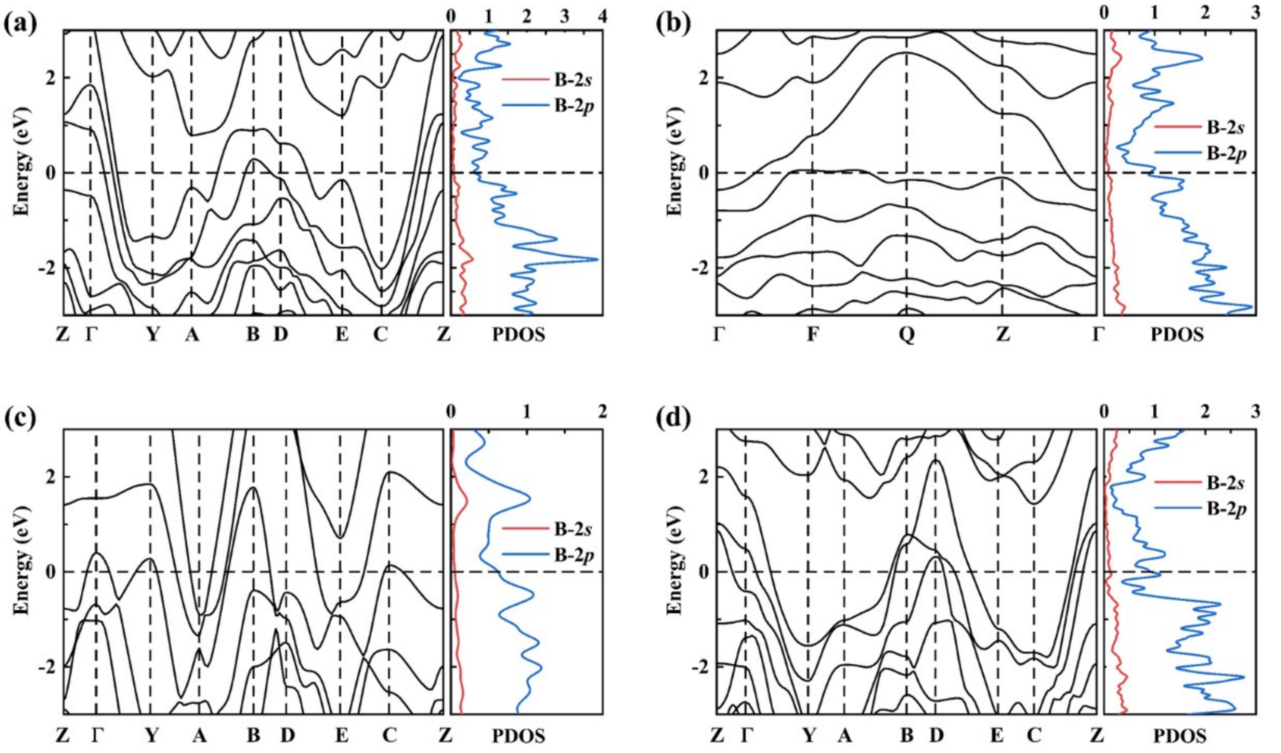

Figure S6. Band structures and density of states (PDOS) of (a) *Pm*_1 B_{12}, (b) *P*1 B_{12}, (c) *P*2/*m* B_6 and (d) *Pm*_2 B_{12} at 0 GPa.

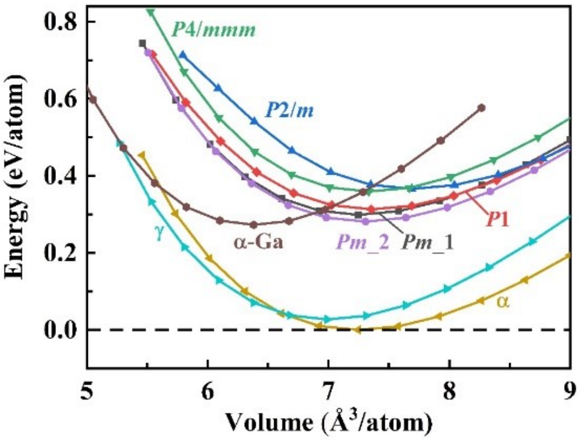

Fig. S7. Energy vs volume curves of various B phases.

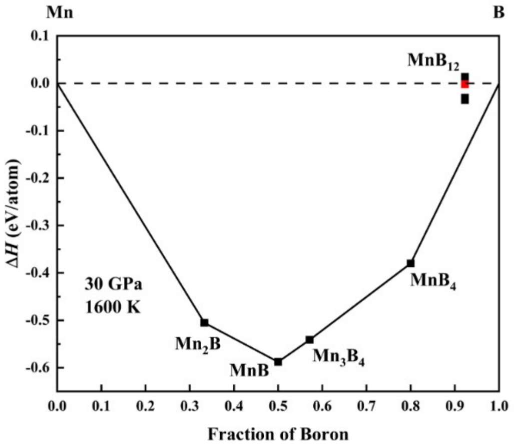

Figure S8. The convex hull diagrams for the Mn-B system at 30 GPa and 1600 K. The red and black solid square represents *t*-MnB_{12} and other $MnB_{12,}$ respectively.

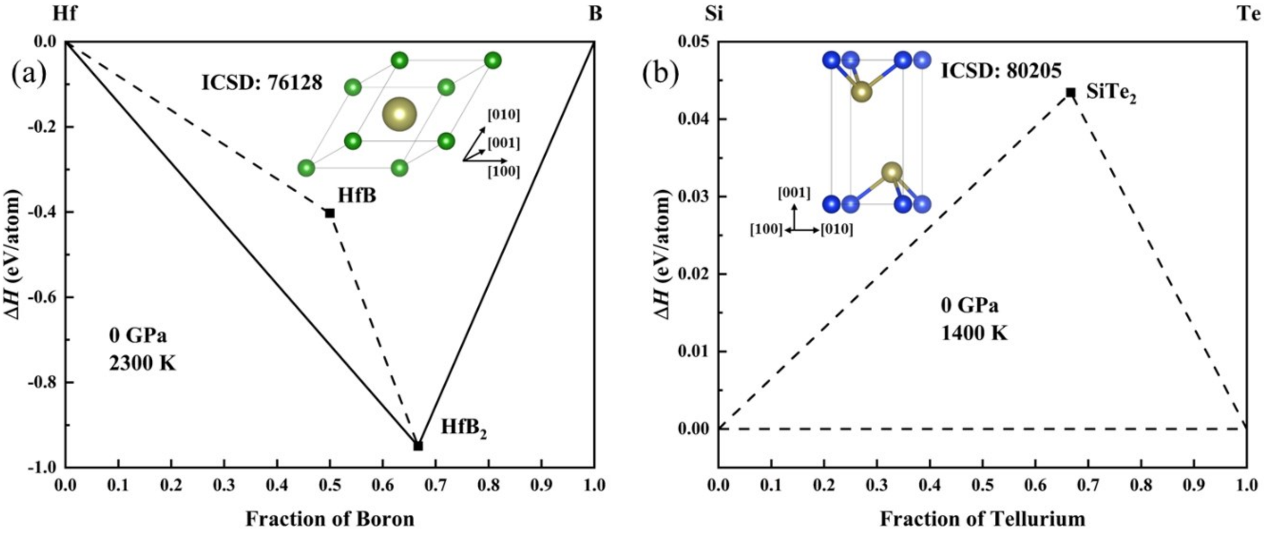

Figure S9. (a) The formation energies of HfB and HfB_2 with respective to hcp-Hf and α-B_{12} at 0 GPa and 2300 K. (b) The formation energies of $SiTe_2$ relative to trigonal Te and cd-Si at 0 GPa and 1400 K.

Table SI. Integrated crystal orbital Hamilton population (ICOHP) of adjacent M-B (M = Mn or Zr), B-B pairs in *t*-MnB_{12}, α-B_{12}, γ-B_{28} and ZrB_{12}.

Phases	Selected Atoms	Average Distance (Å)	Average ICOHP (eV/pair)
t-MnB_{12}	Mn-B	2.30	-0.50
	B-B	2.02	-3.50
α-B_{12}	B-B	1.90	-4.04

γ-B_{28}	B-B	2.30	-2.60
ZrB_{12}	B-B	2.02	-3.56

Table SII. The optimized structural parameters of MnB_{12} compounds at ambient pressure.

Space group	***a*, *b*, *c* (Å, deg)**	**Atomic position**
*Pm*_1	$a = 6.68110$ $b = 2.85570$ $c = 5.20420$ $\alpha = \gamma = 90.0000$ $\beta = 68.9736$	B1(1a) (0.91748 -0.00000 0.70477)
		B2(1a) (0.93471 -0.00000 0.37176)
		B3(1a) (0.15852 -0.00000 0.08765)
		B4(1a) (0.18182 -0.00000 0.44326)
		B5(1a) (0.42117 -0.00000 0.15362)
		B6(1a) (0.40089 -0.00000 0.82482)
		B7(1b) (0.50895 0.50000 0.60613)
		B8(1b) (0.36250 0.50000 0.38379)
		B9(1b) (0.83137 0.50000 0.89378)
		B10(1b) (0.77702 0.50000 0.56260)
		B11(1b) (0.92657 0.50000 0.18068)
		B12(1b) (0.59851 0.50000 0.16848)
		Mn1(1b) (0.16962 0.50000 0.78117)
*P*1	$a = 4.48134$ $b = 4.49023$ $c = 4.67818$ $\alpha = 83.4149$ $\beta = 80.9385$ $\gamma = 81.6565$	B1(1a) (0.69711 0.18216 0.55041)
		B2(1a) (0.98323 0.87854 0.01028)
		B3(1a) (0.36364 0.24723 0.36523)
		B4(1a) (0.98865 0.40430 0.52583)
		B5(1a) (0.92117 0.81046 0.38552)
		B6(1a) (0.43926 0.31917 0.98290)
		B7(1a) (0.82996 0.22855 0.87483)
		B8(1a) (0.29232 0.92109 0.20066)
		B9(1a) (0.27378 0.61563 0.50555)
		B10(1a) (0.06121 0.50793 0.88376)
		B11(1a) (0.52947 0.87311 0.52170)
		B12(1a) (0.35774 0.71768 0.87050)
		Mn1(1a) (0.66780 0.55944 0.19713)
*P*2/*m*	$a = 6.91950$ $b = 2.84700$ $c = 4.85950$ $\alpha = \gamma = 90.0000$ $\beta = 78.9364$	B1(2n) (0.66525 0.50000 0.67663)
		B2(2n) (0.16877 0.50000 0.70084)
		B3(2n) (0.41625 0.50000 0.65884)
		B4(2m) (0.70586 0.00000 0.18161)
		B5(2n) (0.91008 0.50000 0.67666)
		B6(2m) (0.75788 -0.00000 0.81229)
		Mn1(1a) (0.00000 0.00000 0.00000)

	$a = b = 4.14750$	B1(8r) (0.27750	0.72250	0.83578)
$P4/mmm$	$c = 5.30120$	B2(4i) (-0.00000	0.50000	0.65923)
	$\alpha = \beta = \gamma = 90.0000$	Mn1(1b) (0.00000	0.00000	0.50000)
		B1(1b) (0.69409	0.50000	0.57645)
		B2(1a) (0.87967	-0.00000	0.46271)
		B3(1b) (0.48570	0.50000	0.07016)
		B4(1a) (0.16921	-0.00000	0.67833)
	$a = 5.19240$	B5(1a) (0.84919	-0.00000	0.75411)
	$b = 2.86470$	B6(1b) (0.39755	0.50000	0.35912)
*Pm*_2	$c = 6.12050$	B7(1b) (0.72353	0.50000	0.31344)
	$\alpha = \gamma = 90.0000$	B8(1b) (0.35383	0.50000	0.63655)
	$\beta = 101.3702$	B9(1a) (0.22185	-0.00000	0.41486)
		B10(1b) (0.16952	0.50000	0.11529)
		B11(1a) (0.17646	-0.00000	0.95748)
		B12(1b) (0.66077	0.50000	0.84083)
		Mn1(1a) (0.84620	-0.00000	0.09977)
	$a = b = 2.84290$			
t-B	$c = 5.44460$	B1(4i) (0.50000	0.00000	0.83666)
	$\alpha = \gamma = \beta = 90.0000$	B2(2h) (0.50000	0.50000	0.65492)

References

1 P. E. Blöchl, *Phys. Rev. B*, 1994, **50**, 17953–17979.

2 J. P. Perdew, K. Burke and M. Ernzerhof, *Phys. Rev. Lett.*, 1996, **77**, 3865–3868.

3 H. J. Monkhorst and J. D. Pack, *Phys. Rev. B*, 1976, **13**, 5188–5192.

4 R. Dronskowski and P. E. Bloechl, *J. Phys. Chem.*, 1993, **97**, 8617–8624.

5 S. Maintz, V. L. Deringer, A. L. Tchougréeff and R. Dronskowski, *J. Comput. Chem.*, 2016, **37**, 1030–1035.